Korean J. Chem. Eng., **26**(5), 1226-1234 (2009)
DOI: 10.1007/s11814-009-0213-8

Network numerical simulation of two-dimensional nonlinear micropolar hydrodynamics in a Darcian porous medium

Joaquin Zueco*, Osman Anwar Bég,†, and Tong-Bou Chang*****

*ETS Ingenieros Industriales Campus Muralla del Mar, Departamento de Ingenieria Térmica y de Fluidos, Universidad Politécnica de Cartegna, Cartagena, Spain
**Energy Systems, Magnetohydrodynamics and Heat Transfer Research, Mechanical Engineering Subject Group, Department of Engineering and Mathematics, Sheaf Building, Sheffield Hallam University, Sheffield, S1 1WB, England, UK
***Fluid Dynamics and Heat Transfer Research, Department of Mechanical Engineering, Southern Taiwan University, 1 Nai-Tai Street, YungKang City, Tainan County, Taiwan
(*Received 26 January 2009 • accepted 1 March 2009*)

Abstract−The two-dimensional steady-state boundary layer flow of an incompressible micropolar fluid in a Darcian porous medium is studied theoretically and computationally. The governing parabolic partial differential equations are reduced to dimensionless form by using a set of transformations, under appropriate boundary conditions. A network simulation method (NSM) solution is presented. Translational velocities (U, V) are found to increase with a rise in Darcy number (Da) and to increase and decrease, respectively, with a rise in micropolar parameter (Er), i.e., Eringen number (ratio of micropolar vortex viscosity to Newtonian viscosity). Micro-rotation is increased with increasing Er and Da values. Translational velocity gradient, $\partial U/\partial Y$ and micro-rotation gradient, $\partial \Omega/\partial Y$ both increase with Darcy number; however, they are both found to decrease with increasing micropolar parameter, Er. The present study finds applications in polymer flows in filtration systems, chemical engineering, biorheology of porous tissue and plastic sheet processing.

Key words: Non-Newtonian, Micropolar Fluid, Porous Medium, Network Numerical Simulation (NSM), Eringen Number, Darcy Number, Angular Velocity, Rheology

INTRODUCTION

Non-Newtonian flows find numerous applications in petroleum, mechanical, environmental and chemical engineering systems. Food stuff dynamics in industrial systems, polymer gel manufacturing processes and petroleum extraction processes also involve non-Newtonian flow dynamics. Numerous models have been developed to simulate the wide variety of rheological fluids encountered in environmental and industrial systems. These fluids include thixotropic fluids, which have a reversible decrease in shear with time, and rheopetic fluids, which show a reversible increase in shear stress at a fixed shear rate and temperature. Pseudoplastic (shear-thinning) fluids show a decrease in viscosity with increasing shear rate and examples of such fluids are printing inks, biofluids, polymer solutions and melts. Other important categories of non-Newtonian fluids include viscoelastic fluids, which show partial elastic recovery on removal of the deforming stress, and Bingham plastics, which do not flow until a certain critical yield stress is attained. Applications of the Bingham plastic model include polysaccharides that are widely used in foods as thickening, gelling, stabilizing, emulsifying, and water-binding agents. Other examples include metallic oxides, clay-water suspensions (e.g., river sediments), dental creams, paints and thickened hydrocarbon greases. An excellent summary of fundamental rheological flow models is provided in the monograph by Schowalter [1]. Khan et al. [2] studied a new class of biopolymers with unique rheological properties using a pseudoplastic formulation since such functional biopolymers can form very viscous solutions at low concentrations. In the context of novel developments in chemical engineering, other important non-Newtonian fluid models include the Maxwell-Wagner electrorheological model employed by Kim and Kilnberg [3] for activated suspensions. Kang and Sangani [4] employed a bubbly non-Newtonian model and kinetic theory to perform computational simulations for simple shear flows of dilute suspensions of spherical bubbles at large Reynolds numbers, showing that the energy balance contained in bubble velocity fluctuations exerts a significant effect in the rheology of the dispersed phase, which is generally non-Newtonian. Rheological flows are also of importance in polystyrene (PS) and polymethylmethacrylate (PMMA) dynamics. Han et al. [5] employed an advanced rheometric expansion system (ARES) to study storage modulus and loss modulus of the PS and PMMA blends.

In many chemical engineering applications, the regime is frequently a porous medium. Such media are important in drying systems, as described by Amanifard and Haghi [6], fluid-separation technologies, as studied by Kim and Chung [7], processes involving superposed porous saturated media and fluid layers, as elaborated by Kim et al. [8], and hydrogen sulfide biofiltration systems as discussed by Jeong et al. [9]. Yim et al. [10] have studied porous media flows in the context of cake filtration including pre-sedimentation effects using the Ruth equation. Chun et al. [11] have examined the flow of dilute polymer solutions in porous media swelling for potential applications in hydrodynamic chromatography. Lee et al. [12] have investigated the permeation properties in composite

†To whom correspondence should be addressed.
E-mail: O.Beg@shu.ac.uk

mesoporous ceramic membranes showing that permeation performance can be enhanced in the presence of an adsorbing gas species due to the surface diffusion mechanism. Hwang and Choi [13] have analyzed the onset of convection in a porous medium mushy layer during solidification of a binary melt. These studies did not, however, consider rheological flows in porous media. An excellent review of non-Newtonian transport phenomena in porous media up to 1969 was provided by Savins [14]. Kozicki [15] has described in detail a number of rheological flows through principally Darcian packed bed porous media. One of the earliest attempts at producing an accurate transport model for power-law (pseudoplastic/dilatant fluid) liquids flowing through simple porous media systems was presented by Christopher and Middleman [16]. They introduced the concept of a modified permeability defined by using an empirical relationship for the power-law index of the fluid, porosity, the intrinsic permeability and a tortuosity factor. Kemblowski and Michniewicz [17] also studied power-law flow through porous media modifying the Christopher-Middleman relationship. Dharmadikhari and Kale [18] later generalized the earlier studies of Christopher and Middleman [16] and Kemblowski and Michniewicz [17], indicating that the tortuosity factor is velocity-dependent and has lower values for shear-thinning fluids, than Newtonian fluids, due to the shorter path followed by shear-thinning fluids in porous media caused by stretching and contracting deformations of the liquid. An unsteady theoretical study of power-law flow in Darcian regimes was communicated by Pascal [19]. Al-Farris and Pinder [20] studied pseudoplastic transport in Darcian porous materials. Bhargava et al. [21] used the finite element method to analyze the pulsating flow of a Nakamura-Sawada rheological fluid in a porous medium channel. Yoon et al. [22] have investigated the oscillatory thermal convection flow in a horizontal layer of viscoelastic fluid-saturated porous medium, for a wide range of Darcy-Rayleigh numbers. Takhar et al. [23] studied numerically the flow of a third grade elasto-viscous fluid (e.g., polymer) over a flat plate with lateral wall mass flux effects. Bég et al. [24] have further studied thermal convection in dissipative viscoelastic flow in a porous medium.

The above studies have all been confined to rheological fluids which possess constitutive relationships that cannot simulate the micro-structural features of certain complex fluids including oils containing very fine suspensions, physiological fluids (blood containing corpuscles), industrial contaminants containing toxic chemicals, liquid crystal suspensions etc. In chemical engineering, microstructural features are important in, for example, concentrated silica particle suspensions [25], organic/inorganic hybrid nanocomposites based on poly(styrene-butadiene-styrene) copolymer (SBS) and clay which are fabricated by melt intercalation [26] and also microfluid device technologies including the micropacked bed chemical reactor [27]. Eringen [28] introduced an elegant framework for studying the microstructural features of such fluids including couple stresses, gyration, non-deformable rotary motions etc. This so-called micropolar model allows the incorporation of microrotational effects in the fluid rheology and as such can be used to simulate liquids which on a micro-level support surface and also body couples, a feature which is not possible with Navier-Stokes (Newtonian) and even very sophisticated viscoelastic flow models. Significant research in micropolar transport phenomena has therefore resulted owing to great interest in the use of this model in chemical, mechanical and petroleum engineering working fluids. The complexity of the model has, however, necessitated some physical simplifications, which in turn reduce the nonlinearity of the models to be solved. An excellent survey of works up to 1984 is available in the monograph by Stokes [29]. Experimental verification of the micropolar model was confirmed by Migun [30]. The first attempt at developing boundary-layer models for micropolar fluids was made by Peddieson and McNitt [31] who considered a number of classical flows including steady and unsteady flat-plate boundary layers. Later, Gorla [32] analyzed numerically using a shooting method the micropolar boundary layer flow at a stagnation point on a moving wall. Soundalgekar and Takhar [33] presented a comprehensive treatment of the micropolar convection boundary layer flow over a continuously moving plate, showing that micropolar fluids induced cooling in the boundary layer and reduce translational velocity. Several studies mainly of an analytical nature have addressed micropolar flows in porous media, which are important from the viewpoint of filtration of biofluids, cholestoric liquid crystal refinement and also treatment of contaminated oils. Annapurna and Ramaniah [34] studied the unsteady filtration of micropolar fluid through a flat surface. Bernardy [35] used a Darcy model to investigate the transport of micropolar fluid in a porous medium. More recently Bég et al. [36] studied computationally the effects of thermal and species buoyancy and viscous heating on chemically reactive micropolar boundary layers in a Darcian porous medium. Bég et al. [37] also presented the first study of biomagnetic flow in a micropolar-saturated Darcian porous medium using a finite element technique. Bég et al. [38] extended the study in [37] to consider also for the first time the heat transfer in biomagnetic micropolar blood flow though a porous medium using a finite element model. Micropolar convection in a saturated porous medium with thermo-diffusive Soret and Dufour gradient effects was also studied by Bég et al. [39]. In the present study we consider the two-dimensional steady hydrodynamics of micropolar flow past a flat surface adjacent to a Darcian porous regime. A boundary-layer analysis using a drag force formulation for porous effects is utilized. Computations are restricted to a characteristic Reynolds of unity, beyond which the influence of inertia dominates the flow regime and the Darcian model is invalidated. A network numerical solution is presented to elucidate the effects of permeability and also micropolar vortex viscosity expressed, respectively, in terms of Darcy number and an Eringen micropolar number, on linear and angular velocities and also gradients of these functions. Such a study has to the authors' knowledge not received attention in the literature and has important applications in rheological transport modeling in chemical engineering systems.

RHEOLOGICAL CONSTITUTIVE EQUATIONS FOR MICROPOLAR FLUIDS

We consider an incompressible micropolar fluid, for which the gyration tensor, ν_{ij}, can be reduced from nine independent components to three. Such a rheological fluid model possesses the necessary sophistication to simulate accurately the rotary motions of particles suspended in the working fluid of a chemical engineering operation. Micromotion does not incorporate axial contractions or expansions (i.e., stretch is not possible) but comprises solely rotations about the centroid of mass elements. It is a subsection of the micro-

morphic fluid theory [40] in which a more complex microstructure is present. A simple microfluid can support both couples stresses and body moments on an element of fluid. Effectively, the Navier-Stokes fluid theory is extended then to a far more complex fluid theory that is described by not less than nineteen flow conservation equations. These comprise one conservation of mass equation (continuity), three translational momentum equations (which reduce when microstructural effects and couple stresses are neglected, to the classical Navier-Stokes equations), six conservation of microinertia (angular momentum) equations and nine conservation of first stress moment equations. This implies nineteen unknowns and is clearly intractable with the present technologies in computational fluid dynamics, where even solutions of the 3-D Navier-Stokes (elliptic) equations are a challenge. Micropolar theory simplifies the general micromorphic or microfluid theory (also introduced by Eringen [41]) by retaining only the microrotational effects, i.e., such fluids support surface and body couples only. This allows the reduction of the nineteen conservation equations of Eringen micromorphic fluids to just seven equations: the conservation of mass (continuity), three translational momentum equations and three microinertia (angular momentum or "moment of momentum") equations. Hence, points contained within a small element of micropolar fluid can rotate about the centroid of the volume element. It follows that micropolar fluids are a subclass of micromorphic fluids provided that the symmetric part of the first body moment has a special reduced form. They are microfluids which have microisotropic properties. The constitutive equations for a micropolar fluid in vectorial form can therefore be shown to reduce from the general microfluid case to [42]:

Conservation of Mass

$$\frac{\partial \rho}{\partial t}+\nabla\bullet(\rho\chi)=0 \tag{1}$$

Conservation of Translational Momentum

$$(\lambda+2\mu+\chi)\nabla\nabla\bullet\mathbf{V}-(\mu+\chi)\nabla\times\nabla\times\mathbf{V}+\chi\nabla\times\mathbf{N} -\nabla\mathbf{P}+\rho\mathbf{f}=\frac{\partial\mathbf{V}}{\partial t}-\mathbf{V}\times(\nabla\times\mathbf{V})+\frac{1}{2}\nabla\mathbf{V}^2 \tag{2}$$

Conservation of Angular Momentum (Micro-rotation)

$$(\alpha+\beta+\gamma)\nabla\nabla\bullet\mathbf{N}-\gamma\nabla\times\nabla\times\mathbf{N}+\chi\nabla\times\mathbf{V}-2\chi\mathbf{N}+\rho\mathbf{I}=\rho j\ \dot{\mathbf{N}} \tag{3}$$

where **P** is the hydrodynamic pressure and λ, μ, χ, α, β and γ are viscosity coefficients of micropolar fluids, **V**=translational velocity vector, **N** is angular velocity (microrotation) vector and ρ the mass density of micropolar fluid. In the micropolar model theory we are only concerned with two independent kinematical vector fields: the velocity vector field (familiar from Navier-Stokes theory) and the axial vector field which simulates the spin or the microrotations of the micropolar fluid particles, these being assumed non-deformable. We apply this model to the two-dimensional boundary layer flow past a horizontal impermeable surface adjacent to a homogeneous, isotropic Darcian porous medium. Of particular significance in fluid mechanics is the boundary condition at a wall. This is a crucial factor in boundary layer flows. Three conditions are generally of importance in micropolar boundary layer analysis:

a) The limiting lower case of n=0, which corresponds to the case when concentrated particle flows in which the microelements close to the wall surface are unable to rotate.

b) n=0.5, which corresponds to weak micropolarity, i.e., weak concentrations. This has been elucidated by Peddison and McNitt [31] and is of particular relevance to chemical engineering.

c) n=1 is the case for turbulent flows, as shown by Peddieson and McNitt [31]. This is ignored in the present laminar flow study.

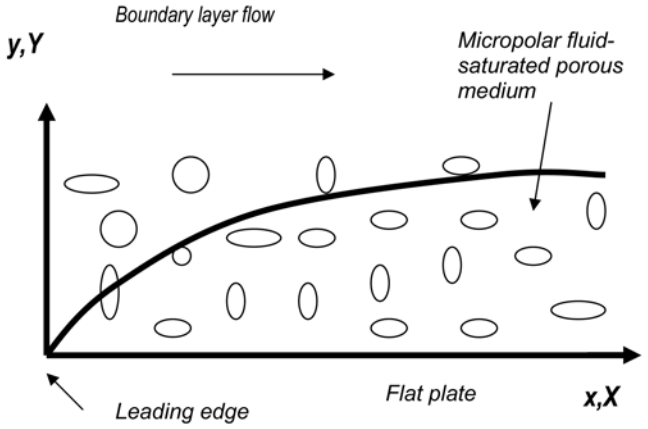

Fig. 1. Micropolar boundary layer flow through a non-Darcian porous medium.

MATHEMATICAL MODEL

The flow regime to be investigated comprises two-dimensional boundary layer flow past a horizontal impermeable surface adjacent to a Darcian porous medium saturated with micropolar liquid, as depicted in Fig. 1. The x-axis is directed along the flow direction and the y-axis normal to this. The porous medium is assumed to be homogeneous and isotropic. The equations governing the steady incompressible flow may be presented as follows:

Mass Conservation (Continuity):

$$\frac{\partial u}{\partial x}+\frac{\partial v}{\partial y}=0 \tag{4}$$

Translational (linear) Momentum:

$$u\frac{\partial u}{\partial x}+v\frac{\partial u}{\partial y}=\left(\nu+\frac{\kappa}{\rho}\right)\frac{\partial^2 u}{\partial y^2}+\frac{\kappa}{\rho}\frac{\partial N}{\partial y}-\left(\nu+\frac{\kappa}{\rho}\right)\frac{1}{K}u \tag{5}$$

Angular Momentum (Micro-rotation):

$$u\frac{\partial N}{\partial x}+v\frac{\partial N}{\partial y}=\frac{\gamma}{\rho j}\frac{\partial^2 N}{\partial y^2}-\frac{\kappa}{\rho j}\left(2N+\frac{\partial u}{\partial y}\right) \tag{6}$$

where all parameters are defined in the notation. We note that in the viscous shear diffusion term, $(\nu+\kappa/\rho)(\partial^2 u/\partial y^2)$, the Newtonian kinematic viscosity is now supplemented by the Eringen micropolar vortex viscosity, κ. These equations are identical to those studied by Gorla [32] with an extra porous media drag force incorporated in Eq. (5). Gorla et al. [32], however, did not solve the full dimensionless version of even the non-porous equations and employed instead a similarity transformation with a stream function formulation. In the present analysis we study the fully nonlinear equations. The appropriate boundary conditions may be specified as:

At the solid boundary:

$$y=0;\ u=v=0,\ N=-\frac{1}{2}\frac{\partial u}{\partial y} \tag{7a}$$

At the free stream:

$$y\to\infty:\ u\to U_0,\ v\to 0,\ N\to 0 \tag{7b}$$

In (7a) the micro-rotation boundary condition at the wall, $N=-1/2\,\partial u/\partial y$, physically implies the vanishing of the anti-symmetric part of the stress tensor and represents weak concentrations of the micro-elements of the micropolar fluid at the solid surface. This is physically valid and has been rigorously analyzed and validated by many researchers including Gorla [32] and Ahmadi [43]. The particle (micro-element) spin is equal to the fluid vorticity at the boundary for fine particle suspensions. For this case, therefore, the microelements are able to sustain rotary motions (although non-vigorous) in the vicinity of the plate. In Eq. (3) the Darcian porous drag force term is defined by the modified term, $-(\nu+\kappa/\rho)(1/K)u$, which is linear in terms of translational velocity, u. With $\kappa=0$ micropolar effects are negated and this body force will reduce to the conventional Newtonian Darcy drag force: $-\nu(1/K)u$. Clearly the micro-rotation component, N, is coupled to the linear momentum Eq. (5) via the angular velocity gradient term, $(\kappa/\rho)(\partial N/\partial y)$. Very strong coupling exists between the translational velocity components, u and v, in Eq. (6) via the convective acceleration terms, $u(\partial N/\partial x)$, $v(\partial N/\partial y)$. Furthermore, there is a second coupling term linking the angular velocity with the x-direction velocity gradient, in Eq. (6): $-(\kappa/\rho j)[2N+(\partial N/\partial y)]$. Eqs. (4) to (6) with boundary conditions (7a, b) constitute a two-point boundary value problem for steady micropolar boundary layer flow in a porous regime. These partial differential equations can further be simplified to non-dimensional form by using a set of non-dimensional transformations. Proceeding with the analysis we define:

$$X=\frac{x}{L},\ Y=y\frac{Re^{1/2}}{L},\ U=\frac{u}{u_c},\ V=v\frac{Re^{1/2}}{u_c},$$
$$\Omega=\frac{NL}{u_c Re^{1/2}},\ Er=\frac{\kappa}{\mu},\ Re=\frac{u_c L}{\nu},\ \lambda=\frac{\gamma}{\mu j},\ \beta=\frac{L\nu}{u_c j},\ Da=\frac{K}{L^2} \tag{8}$$

Implementation of these expressions into the conservation equations leads to the satisfaction of the mass conservation equation, and the following pair of coupled, non-linear partial differential equations in an (X, Y) coordinate system for the non-dimensional translational velocity U, V and micro-rotation, Ω, fields in the porous domain:

Dimensionless Mass Conservation:

$$\frac{\partial U}{\partial X}+\frac{\partial V}{\partial Y}=0 \tag{9}$$

Dimensionless Translational (linear) Momentum:

$$U\frac{\partial U}{\partial X}+V\frac{\partial U}{\partial Y}=[1+Er]\frac{\partial^2 U}{\partial Y^2}+Er\frac{\partial \Omega}{\partial Y}-\frac{1}{DaRe}(1+Er)U \tag{10}$$

Dimensionless Angular Momentum (Micro-rotation):

$$U\frac{\partial \Omega}{\partial X}+V\frac{\partial \Omega}{\partial Y}=\lambda\frac{\partial^2 \Omega}{\partial Y^2}-Er\beta\left(2\Omega+\frac{\partial U}{\partial Y}\right) \tag{11}$$

with corresponding transformed non-dimensional boundary conditions:

At the solid boundary:

$$Y=0:\ U=V=0,\ \Omega=-\frac{1}{2}\frac{\partial U}{\partial Y} \tag{12a}$$

At the free stream:

$$Y\to\infty:\ U\to 1,\ V\to 0,\ \Omega\to 0 \tag{12b}$$

The flow variables are the X-direction and Y-directional translational (linear) velocities, U, V, and the micro-rotation component, i.e., angular velocity of micro-elements, Ω. In physical design applications further quantities based on gradients of these variables are important. These include mass flow per unit width of the surface, M, the momentum flux $M_f(x)$ in the x-direction and also the local wall shear stress, τ_w and local wall couple stress, Γ_w. These are defined, respectively, as follows:

$$M=\int_0^\infty(\rho U)dy \tag{13}$$

$$M_f(x)=\int_0^\infty(\rho U^2)dy \tag{14}$$

$$\tau_w=\left[(\mu+\kappa)\frac{\partial U}{\partial Y}+\kappa\Omega\right]_{Y=0} \tag{15}$$

$$\Gamma_w=\gamma\left[\frac{\partial \Omega}{\partial Y}\right]_{Y=0} \tag{16}$$

NUMERICAL SOLUTIONS

To solve the dimensionless system of Eqs. (9) to (11) with conditions (12a, b) the network simulation method (NSM) is used. This is a very robust, adaptable numerical procedure that has been implemented in many complex chemical and mechanical engineering flow problems by the authors. Bég et al. [44] used NSM to study the unsteady convection boundary layer flow, heat and mass transfer from a vertical surface to a non-Darcian regime with thermal radiation effects. Bég et al. [45] also analyzed the nonlinear thermal convection under buoyancy forces in a thermally stratified porous medium using NSM. Further studies employing NSM include unsteady rotating Couette flow in a Darcy-Forchheimer porous medium [46], transient hydromagnetic dissipative heat transfer in porous media [47], buoyancy-induced double-diffusive radiative convection boundary layers in a porous medium [48], heat-generating hydromagnetic free convection flow from a sphere to a non-Darcian porous regime [49], reactive heat and mass transfer in laminar boundary layer convection from a cylinder to a Darcy-Forchheimer porous medium [50] and thermophoretic particle de- position in magneto-hydrodynamic convection from a moving surface NSM [51]. In the NSM technique, discretization of the differential equations is founded on the finite-difference formulation, where only a discretization of the spatial co-ordinates is necessary, time remaining as a real continuous variable. It is assumed that the electrical variable of voltage is equivalent to the velocities (U, V) and micro-rotation (Ω), while the current is equivalent to the velocity flux ($\partial U/\partial X$, $\partial U/\partial Y$, $\partial V/\partial Y$) and micro-rotation flux ($\partial\Omega/\partial X$, $\partial\Omega/\partial Y$). A network electrical model for each volume element is designed so that its electrical equations are formally equivalent to the spatial discretized equation. NSM can simulate both steady and unsteady flow systems using electric circuits incorporating resistors, capacitors and non-linear devices that seek to resemble thermal systems governed by steady or unsteady linear or non-linear equations. A second-order central difference scheme is used to discretize the flow equations. Once the finite equations have been specified, a network model is designed, whose equations are formally equivalent to the discretized ones. A

number of networks are connected in series to make up the whole medium. Boundary conditions are subsequently added by means of special electrical devices (voltage control-sources or constant voltage sources), i.e., resistors, capacitors etc. The whole network model, including the devices associated with the boundary conditions, is solved by the numerical computer code Pspice [52]. This code imposes and adjusts continuously and automatically the step to reach a convergent solution in each iteration, according to the given stability and convergence requirements. The user does not need to manipulate the finite difference differential equations to be solved nor to pay attention to the convergence problems. Details of the local truncation errors can been found in Nagel [53]. Design of the model, however, requires a comprehensive knowledge of circuit theory. Momentum balance "currents" are defined systematically for each of the discretized equations and errors can be quantified in terms of the quantity of control volumes. To help the user to design the network model and to solve a chemical engineering flow problem by means of NSM, a program in C++ (easy and fast to understand) has been developed, to optimize speed of implementation of the code Pspice (file "Network.cir"). This program generates quickly the file for subsequent execution in Pspice, and the program permits the reading of the solutions provided by Pspice (file "Network.out"). When the simulation is complete, Pspice plots waveform results so the designer can visualize circuit behavior and determine design validity. Graphical results of each simulation are presented in Pspice's Probe window waveform viewer and analyzer, where it is possible to see the translational and angular (micro-rotational) velocity components at any point of the medium. NSM implements the most recent advances in software in the resolution of electrical networks to solve diverse types of partial differential equations which may be elliptical, hyperbolical, parabolic, linear, non-linear, and in 1, 2 or 3 dimensions, all of interest in modern chemical engineering fluid dynamics. To obtain the network model we define the following "currents":

$$J_{U,Y}=\frac{\partial U}{\partial Y} \tag{17}$$

$$J_{U,X}=\frac{\partial U}{\partial X} \tag{18}$$

$$J_{\Omega,Y}=\frac{\partial \Omega}{\partial Y} \tag{19}$$

$$J_{\Omega,X}=\frac{\partial \Omega}{\partial X} \tag{20}$$

With these definitions of the currents, Eqs. (9) and (10) can be cast as follows:

$$UJ_{U,X}+VJ_{U,Y}=(1+Er)\frac{\partial J_{U,Y}}{\partial Y}+ErJ_{\Omega,Y}-\frac{1}{DaRe}(1+Er)U \tag{21}$$

$$UJ_{\Omega,X}+VJ_{\Omega,Y}=\lambda\frac{\partial J_{\Omega,Y}}{\partial Y}-Er\beta(2\Omega+J_{U,Y}) \tag{22}$$

These partial differential equations can be transformed into a system of connected differential equations, by means of the spatial discretization, given by

$$U_{i,j}\frac{(U_{i+\Delta X,j}-U_{i-\Delta X,j})}{\Delta X(1+Er)}+V_{i,j}\frac{(U_{i,j+\Delta Y}-U_{i,j-\Delta Y})}{(1+Er)\Delta Y}=\frac{J_{U_{i,j+\Delta Y}}-J_{U_{i,j-\Delta Y}}}{\Delta Y}$$

$$+Er\frac{\Omega_{i,j+\Delta Y}-\Omega_{i,j-\Delta Y}}{\Delta Y(1+Er)}-\frac{1}{DaRe}U_{i,j} \tag{23}$$

$$U_{i,j}\frac{(\Omega_{i+\Delta X,j}-\Omega_{i-\Delta X,j})}{\Delta X}+V_{i,j}\frac{(\Omega_{i,j+\Delta Y}-\Omega_{i,j-\Delta Y})}{\Delta Y}=\frac{J_{\Omega_{i,j+\Delta Y}}-J_{\Omega_{i,j-\Delta Y}}}{\Delta Y}$$

$$-Er\beta\left[2\Omega_{i,j}+\frac{U_{i,j+\Delta Y}-U_{i,j-\Delta Y}}{\Delta Y}\right] \tag{24}$$

where the following currents (25-28) are implemented by means of resistors of value "ΔY/2" and other currents are implemented with voltage control current generators.

$$J_{U,i,j+\Delta Y}=(U_{i,j+\Delta Y}-U_{i,j})/(\Delta Y/2) \tag{25}$$

$$J_{U,i,j-\Delta Y}=(U_{i,j}-U_{i,j-\Delta Y})/(\Delta Y/2) \tag{26}$$

$$J_{\Omega i,j+\Delta Y}=(\Omega_{i,j+\Delta Y}-\Omega_{i,j})/(\Delta Y/2) \tag{27}$$

$$J_{\Omega i,j-\Delta Y}=(\Omega_{i,j}-\Omega_{i,j-\Delta Y})/(\Delta Y/2) \tag{28}$$

In Eqs. (23) and (24) all the terms can be treated as a current, so if the Kirchhoff law for currents is applied, the network model is obtained. To introduce the boundary conditions a voltage source is employed to simulate constant values of velocity and micro-rotation and a voltage source controlled by voltages is used to simulate the condition at Y=0 for Ω. The NSM method has been extensively validated in many articles by the authors [44-51] with respect to numerous established numerical techniques including for example, finite elements [44], perturbation methods [45], cubic splines [46] and explicit difference methods [47] and therefore we omit comparison solutions here for conservation of space. The method is very dependable and yields extremely accurate solutions. Excellent convergence has been achieved with the NSM model.

RESULTS AND DISCUSSION

A large number of computations have been performed. For conservation of space we have provided only selected results here to illustrate the nature of the flow. The flow equations in dimensionless form are controlled effectively by five parameters: Darcy number (Da), Reynolds number (Re), Eringen number (Er), the spin gradient parameter (λ) and the microinertia parameter (β). Here we study the influence of only Da and Er on flow variables. The other parameters are fixed throughout as β=1, Re=1, λ=1. The present model reduces to purely micropolar flow without porous medium effects when Da$\rightarrow\infty$, i.e., the medium permeability becomes infinite, so that in the limit the Darcian drag becomes vanishingly small. The Newtonian flow case can also be retrieved by setting Er=0, for which micropolar vortex viscosity (κ) becomes zero and the micro-rotation equation vanishes. In this case the translational momentum Eq. (10) reduces to Newtonian boundary layer flow in a Darcian porous medium, defined by:

$$\frac{\partial U}{\partial X}+\frac{\partial U}{\partial Y}=\frac{\partial^2 U}{\partial Y^2}-\frac{U}{DaRe} \tag{26}$$

The values of β=1 and λ=1 used in our computations are representative of micropolar boundary layer flows and imply that spin gradient viscosity and microinertia are constant in the flow regime. These values are accurate for fine polymer suspensions as described in references [32], [33] and [43]. The influence of Darcy number (Da)

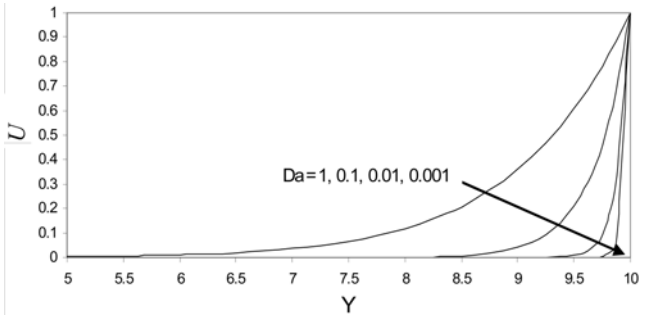

Fig. 2. Variation of X-direction velocity with Y for various Darcy numbers, Da.

on X-direction translational velocity, U, is shown in Fig. 2. A rise in Da from 0.001 through 0.01, 0.1 to 1 (very high permeability) clearly induces a marked rise in U values, i.e., accelerates the flow. The changes in velocity are maximized some distance from the wall, towards the free stream, at Y~9. As such the fluid acceleration towards the edge of the boundary layer is less impeded by wall effects here. As Da increases, the Darcian drag force decreases, due to the inverse relationsip in Eq. (10); porous drag force is therefore progressively lowered with an increase in permeability, i.e., Darcy number, which serves to increase flow velocity, U in the regime. Velocities all rise monotonically from 0 at the wall (no-slip condition) to the maximum value of unity in the free stream (Y=1), with the most gradual ascent accompanying the highest permeability case. High permeabilities would correspond to highly porous industrial materials such as ceramic foams, sparsely packed bed materials etc.

Fig. 3 depicts the effect Eringen number, Er, on translational velocity, U versus Y. We observe that a small increase in U occurs with a considerable increase in Er from 0 (Newtonian case) to 10. From Er=0.1 to Er=1 an almost negligible alteration in U is witnessed. For Er>1, micropolar vortex viscosity exceeds Newtonian dynamic viscosity i.e. $\kappa>\mu$. For Er<1, Newtonian viscosity exceeds micropolar vortex viscosity i.e. $\kappa<\mu$. For Er=1, $\kappa=\mu$. With increasing micropolarity, i.e., larger Er values, translational velocity is therefore boosted, testifying to the usefulness of micropolar fluids in lubrication applications. Flow is accelerated with increasing micropolar vortex viscosity. The micropolar fluid, therefore, has a higher translational velocity than a Newtonian fluid, in the direction parallel to the plate. This is of great significance in polymeric processing since polymer suspensions have been found to flow faster owing to addi-

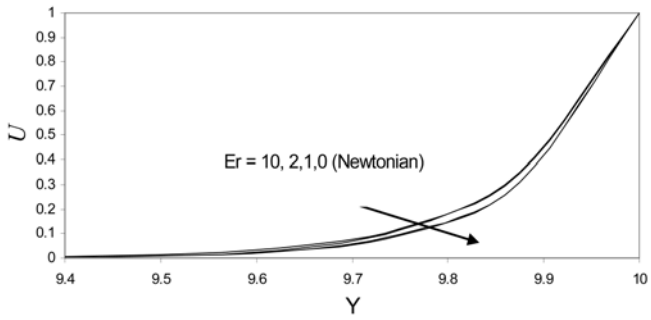

Fig. 3. Variation of X-direction velocity with Y for various Eringen numbers, Er.

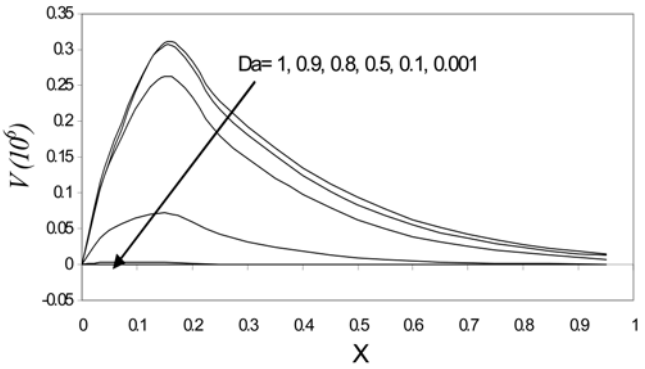

Fig. 4. Variation of Y-direction velocity with X for various Darcy numbers.

tives compared with Newtonian fluids. The micropolar theory, therefore, accurately predicts this characteristic of for example lubricants, contaminated oils, greases etc.

Fig. 4 shows the influence of Darcy number (Da) on the Y-direction translational velocity component, V, wth distance along the plate i.e. X . An increase in Da from 0.001, 0.1, 0.5, 0.8, 0.9 to 1 (very high permeability) causes a significant increase in the velocity component, V. The values of V, however, are much smaller compared with U values (Fig. 3), since the primary flow in the boundary layer is in the X-direction. Darcian drag directly affects the X-direction momentum equation via the term, U/(DaRe) in Eq. (10). As such the Y-direction velocity component (V) which is coupled to the U component via the convective (acceleration term),V ∂U/∂Y, in Eq. (10) is influenced indirectly via the effects felt by the U velocity component. As such, the velocity V has significantly lower values (several orders of magnitude) than U over the same range of Da numbers (Fig. 2). For example, the peak value of V corresponding to the maximum value of Da, i.e., 1, is approximately 0.31×10^{-6}, located at X~0.17. The peak value of U for the same value of Da is, however, much higher and equal to unity. Therefore, even though increasing Da does increase V magnitudes, for a similar argument to why U values are increased (a decrease in Darcian resistance), the increases are extremeley small. In the context of boundary-layer theory, Schlichting [54] has shown that the dominant velocity will be the X-component for flat plate boundary layer flow. Our results

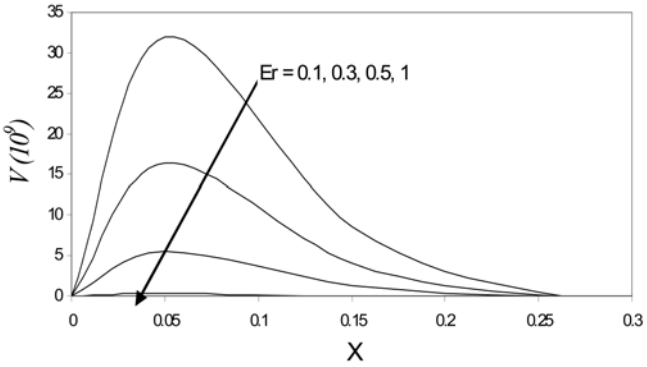

Fig. 5. Variation of Y-direction velocity with X for various Eringen numbers.

show that even for micropolar flows, X-direction momentum does indeed dominate the flow adjacent to the boundary layer so that U velocities are far greater than V velocities.

Fig. 5 shows the influence of Eringen number, Er, on translational velocity, V versus X coordinate. Contrary to the U response, we find that an increase in micropolarity, i.e. ,a rise in Er from 0.1 through 0.3, 0.5 and to 1 (micropolar vortex viscosity equal to Newtonian dynamic viscosity) actually decreases the magnitude of the V component. Peak V value drops, therefore, from 32×10^{-9} for Er=0.1 (very low micropolarity) to almost zero for Er=1. We note again that there is greater coupling between the X-direction velocity and dimensionless micro-rotation, as testified to by the presence of the term, $-Er\beta(2\Omega+(\partial U/\partial Y))$, in the dimensionless micro-rotation Eq. (11) and in the convective acceleration term, $U(\partial\Omega/\partial X)$. Although of course there is also coupling with the V velocity component, this arises only in the convective acceleration terms in (11): $V(\partial\Omega/\partial Y)$. Micropolarity will, therefore, exert a stronger influence on U component than V component of linear velocity, as shown in our results.

The effects of Da and Er on the micro-rotation component, Ω with distance from the wall i.e. Y-coordinate, are shown in Figs. 6 and 7. Clearly, an increase in Da induces a significant rise in micro-rotation component, Ω. With an increase in Da, the permeability of the regime is enhanced, allowing greater space for micro-elements in which to sustain rotations. Micro-rotation (angular velocity) is therefore reduced when Da, i.e., permeability is decreased. Consistent with this we observe that the lowest value of Ω corresponds to the least value of Da. It is also apparent that Ω values remain unaffected for some distance away from the wall, i.e., only when Y reaches about 4 do profiles become non-zero and begin to diverge considerably. Micro-rotation, Ω, is therefore clearly suppressed at the wall, for which Fig. 6 shows that Ω values are zero. With further separation from the wall, i.e., plate, the fluid microelements are able to rotate more freely and with the increase in permeability there is a strong increase for the remainder of the range. Values peak in all cases of Da at for from the plate after which they descend rapidly to zero in the free stream. An increase in micropolar parameter, Eringen number, Er, as seen in Fig. 7, significantly increases micro-rotation values. Clearly, therefore, angular velocity of the micropolar fluid is increased with an increase in micropolar vortex viscosity. Again, we note that micro-rotation values are largely unaffected until some considerable distance from the wall, since the presence of a boundary inhibits rotary motions and stifles micro-rotation values.

Figs. 8 and 9 illustrate the effects of Darcy number, Da, on the X-direction translational velocity gradient ($\partial U/\partial Y$) and micro-rotation gradient ($\partial\Omega/\partial Y$), parameters which are representations of wall shear stress and wall couple stress. In Fig. 8 we observe that a rise in Da has a profound effect on the profiles of $\partial U/\partial Y$ versus X, the distance along the plate. With an increase in Da, translational velocity is increased (as shown in Fig. 2) and as a result the flow is accelerated strongly in the direction along the plate. This boosts the velocity gradient, i.e., increases shear stress at the plate. The micro-rotation gradient ($\partial\Omega/\partial Y$), as shown in Fig. 9, is seen to increase markedly with a rise in Darcy number, Da. The peak value of $\partial\Omega/\partial Y$ is minimized for the lowest value of Da, i.e., 0.001. We observe

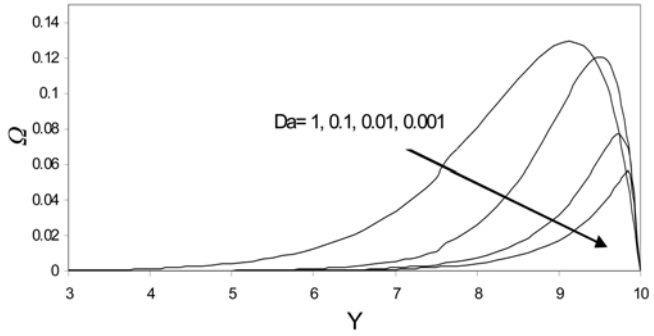

Fig. 6. Variation of micro-rotation (angular velocity) with Y for various Darcy numbers.

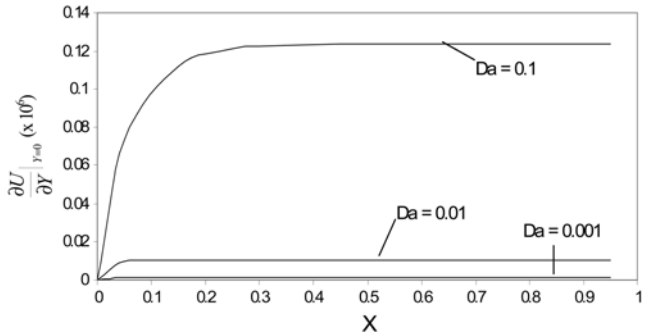

Fig. 8. Variation of translational velocity gradient at the wall with X for various Darcy numbers.

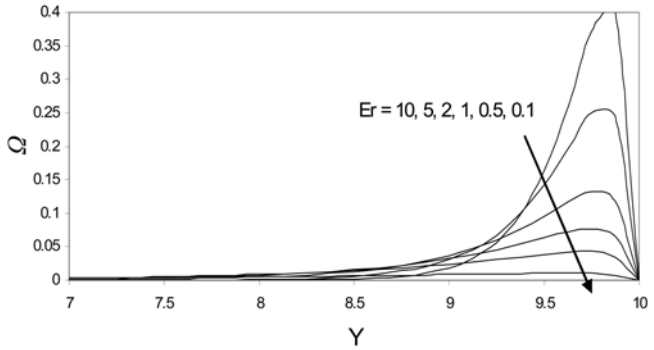

Fig. 7. Variation of micro-rotation (angular velocity) with Y for various Eringen numbers.

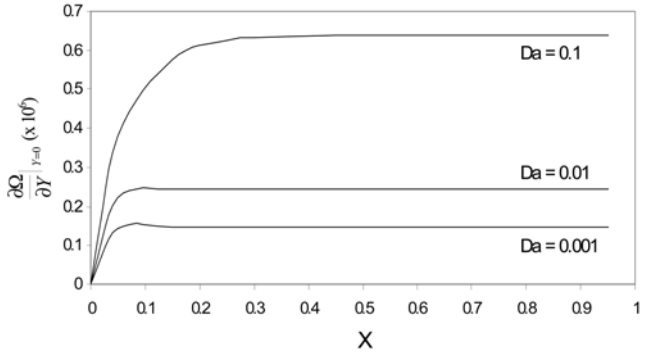

Fig. 9. Variation of micro-rotation gradient at the wall with X for various Darcy numbers.

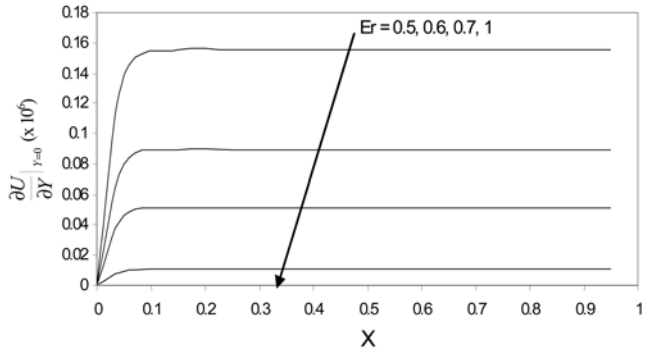

Fig. 10. Variation of translational velocity gradient at the wall with X for various Eringen numbers.

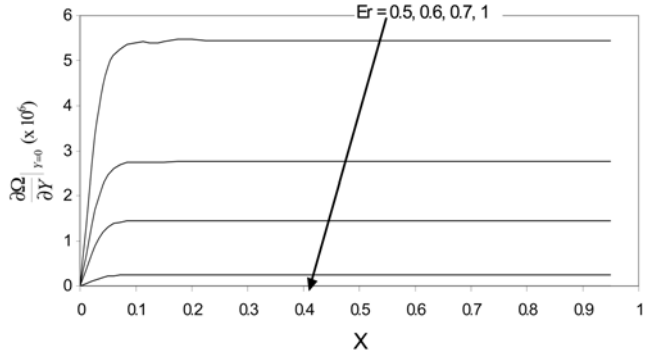

Fig. 11. Variation of micro-rotation gradient at the wall with X for various Eringen numbers.

that all micro-rotation gradient profiles shoot up from zero at the leading edge of the boundary layer (X=0) and rapidly become steady very close to the leading edge full stop. All profiles on attaining the maximum value, stay constant for the remaining length of the plate.

The variation of X-direction translational velocity gradient (∂U/∂Y) and micro-rotation gradient ($\partial\Omega/\partial$Y), with distance along the plate, for various micropolar parameters, i.e., Eringen number (Er), are shown in Figs. 10 and 11. Velocity gradient, ∂U/∂Y, is seen to decrease considerably as Er rises from 0.5 through 0.6, 0.7 to 1. All profiles ascend quickly from zero at the leading edge (X=0) and become steady for the remaining length of the plate. Peak values are attained at X~0.1 and these stay constant along the plate length. From Fig. 11 we observe that an increase in Er value also decreases micro-rotation gradient, ($\partial\Omega/\partial$Y), although values are considerably higher than for velocity gradient (Fig. 10). As a result wall couple stress, $\Gamma_w=\gamma[\partial\Omega/\partial Y]_{Y=0}$ defined in Eq. (16), will also be decreased. The peak value of ($\partial\Omega/\partial$Y), falls from 5.5×10^{-6} for Er= 0.5 to 0.25×10^{-6} for Er=1. Overall, the micropolar fluid is seen to be accelerated along the plate (as seen in Fig. 3) compared with a Newtonian fluid. Hence, the intrinsic rotary motion of micro-elements aids in momentum development explaining the enhanced performance of lubicants containing derivatives compared with Newtonian fluids [14], [16], i.e., micropolarity reduces drag effects. The present computational solutions have been obtained with very high efficiency and are being extended to consider the effect of species diffusion (e.g., Hydrogen gas) in chromatographic gel operations. NSM therefore demonstrates excellent potential for advanced non-Newtonian transport problems in chemical engineering operations.

CONCLUSIONS

A mathematical model has been presented for the two-dimensional, laminar, incompressible, micropolar flow in a porous regime using boundary-layer theory. The equations of mass, linear and angular momentum conservation have been transformed with appropriate boundary conditions. The case of weak microlement concentration at the boundary is considered. Expressions for momentum flux, mass flow per unit width, local wall shear stress and also local wall couple stress are presented. We have computed effects of Darcy number and Eringen number for Re=1 (valid for the limit of Darcy's law, as discussed by Bear [55]) on flow variables. It has been shown that:

i) Increasing Da increases both U and V components of translational velocity

ii) Increasing Da increases micro-rotation, i.e., angular velocity component (Ω)

iii) Increasing Er increases the U translational velocity component and micro-rotation (Ω) but decreases the V translational component of velocity (normal to the wall).

iv) Increasing Da increases both translational velocity gradient (∂U/∂Y) and micro-rotation gradient ($\partial\Omega/\partial$Y) at the wall

v) Increasing Er causes a decrease in both translational velocity gradient (∂U/∂Y) and micro-rotation gradient ($\partial\Omega/\partial$Y) at the wall.

The present study is also currently being extended to consider the effect of variable spin gradient and also transient effects. The results of these investigations will be communicated in the near future.

ACKNOWLEDGMENTS

The authors wish to express their gratitude to the reviewer for his positive comments which we believe have served to considerably improve our article.

NOMENCLATURE

x : coordinate parallel to plate (streamwise)
y : coordinate transverse to plate (spanwise)
u, v : translational velocity components in the (x, y) directions
μ : Newtonian dynamic viscosity
ν : Newtonian kinematic viscosity
κ : vortex viscosity (rotational viscosity) coefficient
ρ : density of the micropolar fluid
N : angular velocity (micro-rotation component in the x-y plane)
K : permeability of porous medium
j : Eringen micro-inertia per unit mass (micro-inertia density)
γ : spin gradient viscosity (gyroviscosity) coefficient
X : dimensionless x coordinate
Y : dimensionless y coordinate
U : dimensionless x-direction translational velocity
V : dimensionless y-direction translational velocity
Ω : dimensionless micro-rotation (angular velocity)
Er : Eringen micropolar number (vortex viscosity: newtonian dynamic viscosity)
Re : characteristic Reynolds number
u_c : characteristic velocity

λ : spin gradient parameter
β : microinertia parameter
Da : Darcy number
L : reference scale length

REFERENCES

1. W. R. Schowalter, *Mechanics of non-newtonian fluids*, Pergamon, New York (1979).
2. T. Khan, J. K. Park and J. H. Kwon, *Korean J. Chem. Eng.*, **24**, 816 (2007).
3. Y. D. Kim and D. J. Klingenberg, *Korean J. Chem. Eng.*, **14**, 30 (1997).
4. S.-Y. Kang and A. A. Sangani, *Korean J. Chem. Eng.*, **19**, 363 (2002).
5. M. S. Han, H. C. Jung, J. H. Park and W. M. Kim, *Korean J. Chem. Eng.*, **19**, 337 (2002).
6. N. Amanifard and A. K. Haghi, *Korean J. Chem. Eng.*, **25**, 191 (2008).
7. K. H. Kim and C. H. Chung, *Korean J. Chem. Eng.*, **18**, 796 (2001).
8. D.-S. Kim, E. S. Cho and C.-K. Choi, *Korean J. Chem. Eng.*, **11**, 190 (1994).
9. G. T. Jeong, G.-Y. Lee, J. M. Cha and D. H. Park, *Korean J. Chem. Eng.*, **25**, 118 (2008).
10. S. S. Yim, Y. D. Kwon and H. I. Kim, *Korean J. Chem. Eng.*, **18**, 741 (2001).
11. M. S. Chun, O. O. Park and J. K. Kim, *Korean J. Chem. Eng.*, **7**, 126 (1990).
12. H. L. Lee, H. Suda and K. Haraya, *Korean J. Chem. Eng.*, **22**, 721 (2005).
13. I. G. Hwang and C. K. Choi, *Korean J. Chem. Eng.*, **25**, 199 (2008).
14. J. G. Savins, *Ind. Eng. Chem*., **61**, 18 (1969).
15. W. Kozicki, *Encyclopedia of Fluid Mechanics*, **5**, 965 (1986).
16. R. H. Christopher and S. Middleman, *I & EC Fundamentals*, **4**, 422 (1965).
17. Z. Kemblowski and M. Michniewicz, *Rheologica Acta*., **18**, 730 (1979).
18. R. V. Dharmadikhari and D. D. Kale, *Chem. Eng. Sci.*, **40**, 527 (1985).
19. H. Pascal, *Int. J. Eng. Sci*., **21**, 199 (1983).
20. T. Al-Farris and K. L. Pinder, *Canadian J. Chem. Eng.*, **65**, 391 (1987).
21. R. Bhargava, H. S. Takhar, S. Rawat, T. A. Bég and O. A. Bég, *Nonlinear Analysis: Modeling and Control J*., **12**, 317 (2007).
22. D. Y. Yoon, M. C. Kim and C. K. Choi, *Korean J. Chem. Eng.*, **20**, 27 (2003).
23. H. S. Takhar, R. Bhargava, S. Rawat, T. A. Bég and O. A. Bég, *Int. J. Appl. Mech. and Eng.*, **12**, 215 (2007).
24. O. A. Bég, H. S. Takhar, R. Bharagava, S. Rawat and V. R. Prasad, *Physica Scripta: Proc. Royal Swedish Academy of Sciences*, **77**, 1 (2008).
25. J.-H. So, W. K. Oh and S. M. Yang, *Korean J. Chem. Eng.*, **21**, 921 (2004).
26. Y. T. Lim and O. O. Park, *Korean J. Chem. Eng.*, **18**, 21 (2001).
27. S. Koo, *Korean J. Chem. Eng.*, **23**, 176 (2006).
28. A. C. Eringen, *J. Mathematics and Mechanics*, **16**, 1 (1966).
29. V. K. Stokes, *Theories of fluids with microstructure: An introduction*, Springer, New York/Berlin (1984).
30. N. P. Migun, *J. Engineering Physics (USSR)*, **41**, 832 (1981).
31. J. Peddieson and P. R. McNitt, *Boundary-layer theory for a micropolar fluid, recent advances in engineering science*, Editor: A. C. Eringen, 5, 1, 405-426, Gordon and Breach, New York (1968).
32. R. S. R. Gorla, *Int. J. Eng. Sci.*, **25**, 759 (1987).
33. V. M. Soundalgekar and H. S. Takhar, *Int. J. Eng. Sci.*, **21**, 961 (1983).
34. N. Annapurna and G. Ramaniah, *Japan J. Appl. Physics*, **15**, 2441 (1976).
35. T. Bernardy, *Vodohospod. Cas*., **28**, 319 (1980).
36. O. A. Bég, R. Bhargava, S. Rawat, H. S. Takhar and T. A. Bég, *Nonlinear Analysis: Modeling and Control J*., **12**, 157 (2007).
37. O. A. Bég, T. A. Bég, H. S. Takhar, R. Bharagava and T.-K. Hung, *Int. J. Fluid Mechanics Research*, **34**, 403 (2007).
38. O. A. Bég, R. Bhargava, S. Rawat, K. Halim and H. S. Takhar, *Meccanica*, **43**, 391 (2008).
39. O. A. Bég, R. Bhargava, S. Rawat and E. Kahya, *Emirates J. Eng. Res.*, **13**, 51 (2008).
40. A. C. Eringen, Mechanics of Micromorphic Continua, Mechanics of Generalized Continua, E. Kroner (Editor), Springer-Verlag, Berlin, 18-35 (1968).
41. A. C. Eringen, *Int. J. Eng. Sci.*, **2**, 205 (1964).
42. G. Nath, *Rheologica Acta*, **14**, 850 (1975).
43. G. Ahmadi, *Int. J. Eng. Sci.*, **14**, 639 (1976).
44. O. A. Bég, J. Zueco, H. S. Takhar and T. A. Bég, *Nonlinear Analysis: Modelling and Control J*., **13**, 281 (2008).
45. O. A. Bég, J. Zueco and H. S. Takhar, *Int. Communications Heat Mass Transfer*, **35**, 810 (2008).
46. O. A. Bég, H. S. Takhar, J. Zueco, A. Sajid and R. Bhargava, *Acta Mechanica*, **200**, 129 (2008).
47. O. A. Bég, J. Zueco and H. S. Takhar, *Communications in Nonlinear Science Numerical Simulation*, **14**, 1082 (2009).
48. O. A. Bég, J. Zueco, T. A. Bég and H. S. Takhar, *Acta Mechanica*, **202**, 181 (2009).
49. O. A. Bég, J. Zueco, R. Bhargava and H. S. Takhar, *Int. J. Thermal Sciences*, **48**, 913 (2009).
50. J. Zueco, O. A. Bég, T. A. Bég and H. S. Takhar, *J. Porous Media*, **12**, 519 (2008).
51. J. Zueco, O. A. Bég, H. S. Takhar and V. R. Prasad, *Applied Thermal Engineering*, **29**, 2808 (2009).
52. Pspice 6.0. Irvine, California 92718. Microsim Corporation, 20 Fairbanks (1994).
53. L. W. Nagel, SPICE, Computer Program to Simulate Semiconductor Circuits, Memorandum UCB/ERL M520, University of California, Berkeley, USA (1975).
54. H. Schlichting, *Boundary-layer theory*, McGraw-Hill, New York, 6^{th} edition (1979).
55. J. Bear, *Dynamics of fluids in porous media*, Dover, New York (1988).